

Double perovskite $\text{Ba}_2\text{CdReO}_6$: a ferromagnetic topological semi-half-metal with coexistence of Weyl and nodal-ring states

Xinlei Zhao¹, Fengjie Ma^{1,*} and Zhong-Yi Lu²

¹*The Center for Advanced Quantum Studies and Department of Physics,
Beijing Normal University, 100875 Beijing, China and*

²*Department of Physics, Renmin University of China, Beijing 100872, China*

(Dated: August 3, 2020)

Magnetic topological quantum materials have attracted great attention due to their exotic topological quantum physics induced by the interplay among crystallography, magnetism, and topology, which are of profound importance to fundamental research and technology applications. However, limited materials are experimentally available, most of whom are realized by magnetic impurity doping or heterostructural constructions. In this work, based on the first-principles calculations, we predict that double perovskite $\text{Ba}_2\text{CdReO}_6$ is an intrinsic ferromagnetic topological semi-half-metal with a pair of Weyl points and fully spin-polarized nodal-ring states in the vicinity of the Fermi level. Its two-dimensional nearly flat drumhead surface states are completely spin-polarized, which would provide a wonderful platform to study the emerging intriguing properties, especially for the applications in spintronics, information technology, and topological superconductivity.

I. INTRODUCTION

Topological materials have great potential in many frontier fields due to the existence of nontrivial topological quantum states and have become a hot topic in material science and condensed matter physics^{1–10}. Recently, the discovery of time-reversal breaking magnetic topological materials that have exotic properties beyond non-magnetic topological systems, opens a new burgeoning field and attracts more and more attention^{11–24}. Magnetic topological materials have many advantages due to the interplay between magnetism and topology that offers an imaginative degree for exploring the emerging topological quantum physics, which are of profound importance to fundamental research and technology applications. For example, topological axion states were predicted to exist at the surface of a three-dimensional antiferromagnetic topological insulators^{25,26}; quantized anomalous Hall effect can be achieved in intrinsic ferromagnetic Weyl semimetals without an external magnetic field²⁷; and the emergence of Majorana modes with non-Abelian statistics in the edge/corner states of magnetic topological materials is closely associated with topological superconductivity and relevant for topological quantum computations^{28,29}. Great effort has been devoted in the search of new magnetic topological quantum materials. However, only very few limited materials are experimentally available, most of whom are realized by magnetic impurity doping or heterostructural constructions that are quite challenging for industry^{18,20,30–32}.

Magnetic topological semimetals are of particular important in magnetic topological materials, since quantum transport, spin dynamics, magnetism, as well as topology are all correlated in these systems. The spin polarized valence and conduction bands of magnetic topological semimetals are linearly intersected due to nontrivial topology, forming zero dimensional discrete points or one dimensional continuum curves with nontrivial topological numbers around the Fermi level^{33,34}. In addi-

tion to the advantages of regular topological materials, the high mobility carriers with readily manipulative spins through external fields and disentangled distinctive topological states near the Fermi level could result in exotic transport and spectroscopic behaviors.

Recently, topological nodal-line spin-gapless semi-metals (TNLSGSMs) are proposed as a new type of topological quantum materials with coexistence of spin-fully-polarized and linearly dispersed nodal-line states in the vicinity of the Fermi level¹⁴. Two-dimensional drumhead surface states are considered to be the fingerprint of topological nodal-line semi-metals. They usually lie in the mirror plane of Brillouin zone (BZ) protected by the mirror symmetry and produce a large surface density of states^{34,35}. The two-dimensional drumhead surface states in TNLSGSMs are completely spin polarized, which would be greatly beneficial to spintronics and equal spin-pairing topological superconductivity¹⁴. However, TNLSGSMs are rarely realized experimentally. One main reason is that ferromagnetic semi-metals are very rare in nature, regardless of its topological trivial/nontrivial character. In addition, the nodal-lines in semi-metals are normally deformed into discrete points or fully gapped in the present of spin-orbit coupling (SOC). There are only few materials with $R\bar{3}c$ space group symmetry were predicted to be TNLSGSMs that are stable against SOC¹⁴.

In this paper, we predict that the double perovskite (DP) $\text{Ba}_2\text{CdReO}_6$, compound with space group symmetry $Fm\bar{3}m$, is a new type of intrinsic ferromagnetic TNLSGSM by first-principles calculations. DP has a general chemical formula of $A_2\text{BB}'\text{O}_6$, where A-site cation represents alkaline earth or rare earth element, and B/B' is a cation of transition metal, alkali metal, alkaline earth, or main group metal element. Due to the flexible combination of magnetic or non-magnetic B and B' ions, the DP $A_2\text{BB}'\text{O}_6$ family exhibits various crystal structures, rich electronic properties, and abundant magnetic structures. The barium based compound $\text{Ba}_2\text{CdReO}_6$

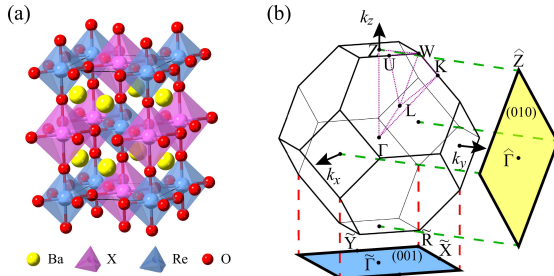


FIG. 1. (a) Crystal structure of DP $\text{Ba}_2\text{CdReO}_6$ with $Fm\bar{3}m$ space group symmetry. (b) The bulk Brillouin zone (BZ) of $\text{Ba}_2\text{CdReO}_6$ with high symmetry points labeled. The projected surface BZs of (001) and (010) planes are depicted by blue and yellow semitransparent planes, respectively.

has been experimentally synthesized before³⁶. However, there is no experimental study about the magnetism of $\text{Ba}_2\text{CdReO}_6$ yet. Our calculations presented here predict that the ground state of $\text{Ba}_2\text{CdReO}_6$ is ferromagnetic. Moreover, it is an ideal intrinsic ferromagnetic TNLS-GSM. The material possesses a pair of Weyl points and one nodal-ring in the first BZ.

II. COMPUTATIONAL DETAILS

In our calculations, the plane-wave basis based method and Quantum-ESPRESSO software package are used^{37,38}. We adopt the generalized gradient approximation (GGA) of Perdew-Burke-Ernzerhof formula for the exchange-correlation potentials in the electronic structure simulations³⁹. The ultrasoft pseudopotentials are employed to model the electron-ion interactions⁴⁰. A corrective Hubbard-like U term is introduced to treat the strong on-site Coulomb interaction of the localized Re-5d electrons, whose effective value is set to 3.0 eV^{41,42}. Parameter-free *ab-initio* calculations with the recently developed strongly constrained and appropriately normed (SCAN) meta-GGA exchange-correlation functional are also performed for crossing checks, which have been demonstrated to be able to give an accurate descriptions of strongly correlated materials without invoking any free parameters such as the Hubbard U^{43,44}. A mesh of $16 \times 16 \times 16$ k-points grid is used for sampling the BZ, and the marzari-vanderbilt broadening technique is adopted⁴⁵. After full convergence tests, the kinetic energy cutoff for wavefunctions and charge densities are chosen to be 80 and 640 Ry, respectively. During the simulations, all structural geometries are fully optimized to achieve the minimum energy. The surface states are studied using tight-binding methods by the combination of Wannier90⁴⁶ and WannierTools⁴⁷ software packages.

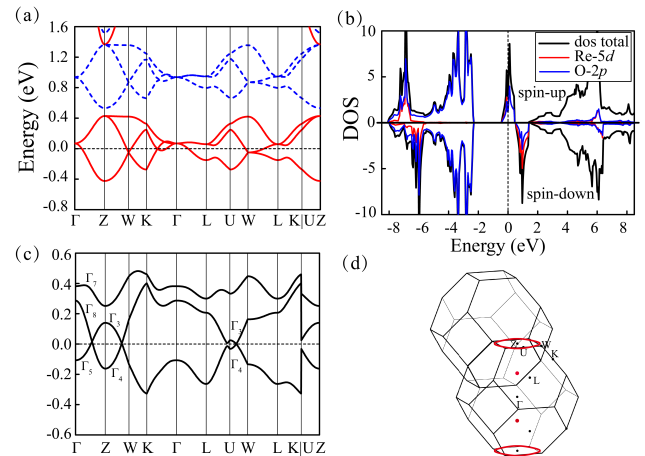


FIG. 2. (a) Band structure of $\text{Ba}_2\text{CdReO}_6$ without SOC in the FM ground state. The up (majority) and down (minority) spin bands are denoted by red solid and blue dashed lines, respectively. (b) Total and orbital-resolved partial density of states of $\text{Ba}_2\text{CdReO}_6$. (c) Band structure of $\text{Ba}_2\text{CdReO}_6$ with SOC included. (d) Distribution of Weyl points and nodal-ring in the bulk BZ. The two red dots represent a pair of Weyl points, whereas the red lines give the nodal-ring.

III. RESULTS AND DISCUSSION

The crystal structure of DP $\text{Ba}_2\text{CdReO}_6$ belongs to an ideal cubic rock-salt type with space group symmetry $Fm\bar{3}m$ (No. 225), as shown in Fig. 1(a). Its unit cell is doubled compared to that of a single perovskite⁴⁸. The corresponding first BZ with high symmetry points is shown in Fig. 1(b). In our calculations, multiple possible magnetic orders of ground states are considered, including antiferromagnetic-I (AFM-I), AFM-II, ferromagnetic (FM), and non-magnetic (NM) states⁴⁹. The calculations reveal that DP $\text{Ba}_2\text{CdReO}_6$ has a FM ground state. If we assume that the energy of FM $\text{Ba}_2\text{CdReO}_6$ is zero, the relative energies of AFM-I, AFM-II, and NM states are 6.4, 19.0, and 120.3 meV per formula unit cell, respectively. After fully relaxation of geometries, the optimized lattice constants are $a=5.95\text{\AA}$ and $c=8.41\text{\AA}$, in good agreement with experiments³⁶. The ordering magnetic moment that is mainly around Re ion with electronic configuration of Re^{6+} ($5d^1, t_{2g}^1$), $\sim 1.0 \mu_B$. Similar results are able to be obtained with the more advanced SCAN meta-GGA functional. Therefore, with the selected U value, our GGA+U calculations can describe the electronic structures of this material very well.

In the absence of SOC, the internal spin space is decoupled from the lattice space. Here we set the moments of Re atoms aligned along z axis. Figure 2(a) gives the band structure of $\text{Ba}_2\text{CdReO}_6$ in the FM ground state, of which the majority spin possesses metallic states while the minority one is insulating. Focusing on the low-energy bands that are well separated from the others, linear dispersions with crossings in the momentum space

TABLE I. The Cartesian coordinates, Chern numbers, and energies (with respect to the Fermi level) of the Weyl points in $\text{Ba}_2\text{CdReO}_6$.

Points	Position (\AA^{-1})	Chern number	$E-E_F$ (meV)
W1	(0, 0, 0.4128)	-1	12
W1'	(0, 0, -0.4128)	1	12

can be observed at W point and between K- Γ in the majority spin channel. The material is therefore a half-semi-metal with completely spin polarization around the Fermi level. This can be also clearly seen from the total and orbital-resolved partial density of states (DOS) of Fig. 2(b). A trivial band gap of ~ 2.86 eV opens in the minority spin channel, whereas the majority one contributes significant states forming a peaklike DOS at the Fermi level, which consist mainly of Re-5d and O-2p orbitals. The material is therefore a promising candidate for applications as spintronics devices.

Once SOC is included in calculations, the two spins couple with each other breaking the spin-rotation symmetry. As we set the moments aligned along z axis, the M_x , M_y , C_{4x} , and C_{4y} symmetries get broken. However, the M_z and C_{4z} symmetries are still preserved. The symmetry of DP $\text{Ba}_2\text{CdReO}_6$ is therefore reduced to D_{4h} (C_{4h}) magnetic point group. The band touching points around the Fermi level are mostly gapped, as shown in Fig. 2(c). Near Γ , the bands split into three bands labeled by Γ_5 , Γ_7 , and Γ_8 according to their different irreducible representations, of which Γ_5 and Γ_8 are linearly intersected forming an isolated zero-dimensional Weyl point between Γ -Z, which is protected by the C_{4z} rotation symmetry. The crossings between Γ -X and Γ -Y directions are opened without any symmetry protection. In $k_z=\pi/c$ plane, there are also two bands intersected linearly with each other along the directions of Z-W and U-W, as labeled by Γ_3 and Γ_4 which belong to the irreducible representations of C_{2v} symmetry. Note that, compared with the band structure of Fig. 2(a) without SOC, the touching points move away from W point. There is no symmetry protecting that the crossings must occur at W point. However, the M_z symmetry ensures that they have to be happened in the same $k_z=\pi/c$ plane. A flat nodal-ring winding around Z point is thus formed, as shown in Fig. 2(d). Within the first bulk BZ, the nodal-ring and the pair of Weyl points are represented by red line and red dots, respectively.

Figures 3(a) and Fig. 3(b) illustrate the energy dispersions of the highest valence and lowest conduction bands of DP $\text{Ba}_2\text{CdReO}_6$ as a function of k in $k_z=\pi/c$ and $k_z=0.5528\pi/c$ planes, respectively. The two bands touch with each other, forming a nodal-ring and Weyl point in the two planes, respectively. Around the Weyl point, the bands always disperse linearly, i.e. along the k_z direction (Γ -Z direction of Fig. 2(c)) and $k_{xy}/k_x/k_y$ directions (left panel of Fig. 3(e)). The valence and conduction bands therefore form a perfect Weyl cone in

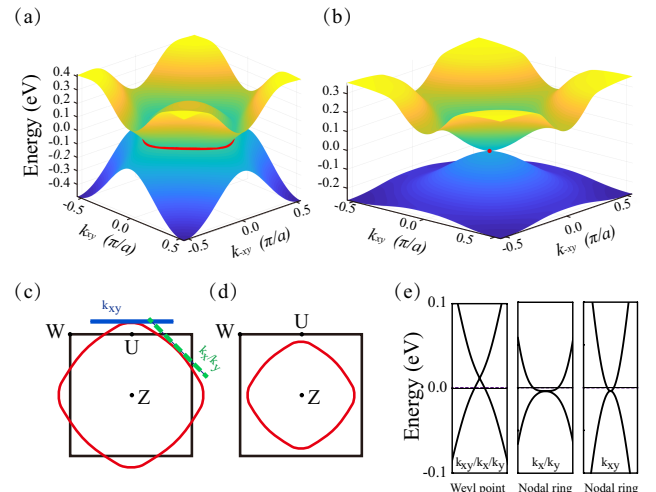


FIG. 3. The energy dispersion of the highest valence band and the lowest conduction band of $\text{Ba}_2\text{CdReO}_6$ as a function of k , forming nodal-ring and Weyl point in the (a) $k_z=\pi/c$ plane and (b) $k_z=0.5528\pi/c$ plane. Color scale indicates the level of energy. Nodal-rings depicted on the boundary plane of BZ are from calculations with different U : (c) $U=3.0$ and (d) $U=5.5$ eV. (e) Left panel shows the band dispersion around the Weyl point along the planar (perpendicular to k_z) directions, whereas the middle and right panels give the dispersions along the two tangent directions of nodal-ring as marked in Fig. 3(c).

the momentum space. Table I lists the Cartesian coordinates, Chern numbers, and relative energies related to the Fermi level of the Weyl points, in which the chiral charges are obtained by integrating the Berry curvature of the sphere surrounding the Weyl points in the momentum space⁵⁰. The relative energies of the Weyl points in $\text{Ba}_2\text{CdReO}_6$ are about 12 meV above than the Fermi level, whereas the nodal-ring states locate slightly below the Fermi level. Interestingly, different with those of Weyl point, the band dispersions of the nodal-ring states are quadratic along k_x/k_y or k_{xy} directions, as shown in the middle and right panels of Fig. 3(e). This character is similar to previous observations in nodal-line Heusler semi-metals, which was thought to be one hallmark of topological nodal-line semi-metals¹³. Note that in most topological nodal-line materials, the nodal-line states are stable only without SOC interaction. They are normally fully gapped or deformed into discrete Weyl points when SOC is considered¹¹. In DP $\text{Ba}_2\text{CdReO}_6$, however, the nodal-ring is stable in the presence of SOC.

We further examined the effect of on-site Coulomb repulsion U , since the bands near the Fermi level are mainly contributed by Re-5d and O-2p orbitals. Different U values ranging from 2.0 eV to 5.5 eV were considered. The bands near the Fermi level are insensitive to the U values used, except that the radius of nodal-ring decreases slightly as U increases, as shown in Fig. 3(c) of $U=3.0$ eV and Fig. 3(d) of $U=5.5$ eV. When U is larger than ~ 5.0 eV, the nodal-ring fully shrinks into the plane of first BZ.

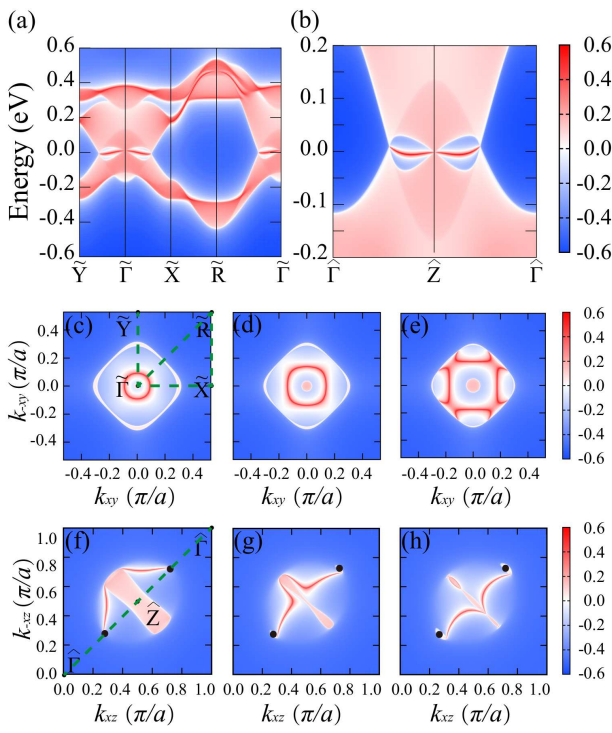


FIG. 4. The surface states of $\text{Ba}_2\text{CdReO}_6$ projected onto (a) (001) surface and (b) (010) surface, of which the energy dispersions are plotted along the green dashed lines marked in (c) and (f), respectively. The evolution of projected surface states and Fermi arc onto (001) and (010) planes at different chemical potentials: (c) 5 meV, (d) 0 meV and (e) -4 meV for (001) surface, and (f) 12 meV, (g) 0 meV, and (h) -4 meV for (010) surface, respectively. The black dots in Fig. (f-h) represent the Weyl points.

There will be no touching point along U-W (edges of first BZ). However, the Weyl point between Γ -Z and crossing between Z-W remain preserved.

The topological surface states of DP $\text{Ba}_2\text{CdReO}_6$ can be obtained with WannierTools software package based on the Green's function method using tight-binding Hamiltonian constructed by the maximally localized Wannier functions^{46,47,51,52}. Figure 4(a) and Fig. 4(b) give the band dispersions projected onto (001) and (010) surfaces, following the high-symmetry k -paths marked by green dashed lines in Fig. 4(c) and Fig. 4(f), respectively. On the projected (001) surface, topological non-trivial surface states are clearly visible, connecting the two gapless points within $\tilde{\Gamma}-\tilde{X}$ and $\tilde{\Gamma}-\tilde{Y}$ and forming a two-dimensional drumhead surface, which is a hallmark of topological nodal-line semimetals^{53,54}. The drumhead states lie in the mirror plane of BZ and are fully spin-polarized. They are protected by the mirror symmetry, producing a large surface density of states. The nearly flat drumhead surface states with complete spin polarization could lead to the equal spin-pairing topological

superconductivity, such as p or f wave topological superconductors, and is greatly beneficial to spintronics¹⁴. As shown in Figs. 4 (c-e), the surface states vary with the chemical potential μ . They form a small ring centered around $\tilde{\Gamma}$ when $\mu=5$ meV (Fermi energy is set to 0). As μ decreases, the size of ring increases initially. When the value of μ is close to the energy of nodal-ring states, the surface states transform into a loop centered around the nodal corners, as shown in Figs. 4 (e). With a further lowering of μ , the surface states becomes smaller and smaller, leaving only the projected bulk states. Since the Weyl points locate along the high-symmetry $-\text{Z}-\Gamma-\text{Z}$ path, there is no Fermi arc connecting the two Weyl points on the projected (001) surface. However, it is visible on the (010) projected surface. As illustrated in Figs. 4(f-h), there exists a Fermi arc that connects two Weyl points with opposite chirality located between $\tilde{\Gamma}-\tilde{\text{Z}}$ of the two adjacent BZs. Part of the Fermi arc merges into projected bulk states including the nodal-ring states. As μ decreases, the projection of bulk states shrinks. When μ equals to the energy of nodal-ring, the projected bulk states are mainly composed of nodal-ring states, resulting in a coexistence of projected nodal-ring and Fermi arc states on the surface of the material, as shown in Fig. 4(h).

IV. CONCLUSION

In summary, we predict that the DP $\text{Ba}_2\text{CdReO}_6$ is an intrinsic FM topological nodal-ring semi-half-metal, in which there coexist a pair of Weyl points along Γ -Z direction and one nodal-ring in the $k_z=\pi/c$ plane of BZ. Different with most of nodal-line materials, the nodal-ring is robust against SOC once the direction of magnetism is perpendicular to the mirror plane. Nearly flat drumhead surface states with complete spin polarization are found in this material, which will produce a large surface density of states around the Fermi level. Our findings therefore provide a wonderful platform for studying the relationship between magnetism and topology, providing a potential high-performance candidate for applications of spintronics and topological superconductivity.

Note added: When submitted the manuscript, we noticed that there was a paper just published in PRB⁵⁵, which studied the topological properties of similar materials and obtained similar results.

V. ACKNOWLEDGMENTS

This work was supported by the National Natural Science Foundation of China under Grants No. 11674027 and 11888101. All calculations were performed at the high performance computing cluster of the Center for Advanced Quantum Studies and Department of Physics, Beijing Normal University, and the National Supercomputer Center in Guangzhou.

* fengjie.ma@bnu.edu.cn

¹ N. P. Armitage, E. J. Mele, and A. Vishwanath, Rev. Mod. Phys. **90**, 015001 (2018).

² H. Gao, J. W. Venderbos, Y. Kim, and A. M. Rappe, Annual Review of Materials Research **49**, 153 (2019).

³ M. Vergniory, L. Elcoro, C. Felser, N. Regnault, B. A. Bernevig, and Z. Wang, Nature **566**, 480 (2019).

⁴ F. Tang, H. C. Po, A. Vishwanath, and X. Wan, Nature **566**, 486 (2019).

⁵ T. Zhang, Y. Jiang, Z. Song, H. Huang, Y. He, Z. Fang, H. Weng, and C. Fang, Nature **566**, 475 (2019).

⁶ S.-Y. Xu, C. Liu, S. K. Kushwaha, R. Sankar, J. W. Krizan, I. Belopolski, M. Neupane, G. Bian, N. Alidoust, T.-R. Chang, *et al.*, Science **347**, 294 (2015).

⁷ T. Liang, Q. Gibson, M. N. Ali, M. Liu, R. J. Cava, and N. P. Ong, Nature Materials **14**, 280 (2015).

⁸ J. Feng, Y. Pang, D. Wu, Z. Wang, H. Weng, J. Li, X. Dai, Z. Fang, Y. Shi, and L. Lu, Physical Review B **92**, 081306 (2015).

⁹ X. Huang, L. Zhao, Y. Long, P. Wang, D. Chen, Z. Yang, H. Liang, M. Xue, H. Weng, Z. Fang, *et al.*, Physical Review X **5**, 031023 (2015).

¹⁰ C.-L. Zhang, S.-Y. Xu, I. Belopolski, Z. Yuan, Z. Lin, B. Tong, G. Bian, N. Alidoust, C.-C. Lee, S.-M. Huang, *et al.*, Nature Communications **7**, 10735 (2016).

¹¹ J. Zou, Z. He, and G. Xu, npj Computational Materials **5**, 1 (2019).

¹² S. Nie, G. Xu, F. B. Prinz, and S.-c. Zhang, Proceedings of the National Academy of Sciences **114**, 10596 (2017).

¹³ G. Chang, S.-Y. Xu, H. Zheng, B. Singh, C.-H. Hsu, G. Bian, N. Alidoust, I. Belopolski, D. S. Sanchez, S. Zhang, *et al.*, Scientific reports **6**, 1 (2016).

¹⁴ R.-W. Zhang, Z. Zhang, C.-C. Liu, and Y. Yao, Physical Review Letters **124**, 016402 (2020).

¹⁵ S. Nie, Y. Sun, F. B. Prinz, Z. Wang, H. Weng, Z. Fang, and X. Dai, Phys. Rev. Lett. **124**, 076403 (2020).

¹⁶ Z. Wang, M. Vergniory, S. Kushwaha, M. Hirschberger, E. Chulkov, A. Ernst, N. P. Ong, R. J. Cava, and B. A. Bernevig, Physical Review Letters **117**, 236401 (2016).

¹⁷ H. Yang, Y. Sun, Y. Zhang, W.-J. Shi, S. S. Parkin, and B. Yan, New Journal of Physics **19**, 015008 (2017).

¹⁸ Q. Wang, Y. Xu, R. Lou, Z. Liu, M. Li, Y. Huang, D. Shen, H. Weng, S. Wang, and H. Lei, Nature Communications **9**, 3681 (2018).

¹⁹ P. Tang, Q. Zhou, G. Xu, and S.-C. Zhang, Nature Physics **12**, 1100 (2016).

²⁰ K. Kuroda, T. Tomita, M.-T. Suzuki, C. Bareille, A. Nugroho, P. Goswami, M. Ochi, M. Ikhlas, M. Nakayama, S. Akebi, *et al.*, Nature Materials **16**, 1090 (2017).

²¹ R. Wang, Y. Jin, J. Zhao, Z. Chen, Y. Zhao, and H. Xu, Physical Review B **97**, 195157 (2018).

²² Y. Xu, Y. Gu, T. Zhang, C. Fang, Z. Fang, X.-L. Sheng, and H. Weng, APL Materials **7**, 101109 (2019).

²³ J.-Y. You, C. Chen, Z. Zhang, X.-L. Sheng, S. A. Yang, and G. Su, Physical Review B **100**, 064408 (2019).

²⁴ H. Li, S.-Y. Gao, S.-F. Duan, Y.-F. Xu, K.-J. Zhu, S.-J. Tian, J.-C. Gao, W.-H. Fan, Z.-C. Rao, J.-R. Huang, J.-J. Li, D.-Y. Yan, Z.-T. Liu, W.-L. Liu, Y.-B. Huang, Y.-L. Li, Y. Liu, G.-B. Zhang, P. Zhang, T. Kondo, S. Shin, H.-C. Lei, Y.-G. Shi, W.-T. Zhang, H.-M. Weng, T. Qian, and H. Ding, Phys. Rev. X **9**, 041039 (2019).

²⁵ R. S. K. Mong, A. M. Essin, and J. E. Moore, Phys. Rev. B **81**, 245209 (2010).

²⁶ D. Zhang, M. Shi, T. Zhu, D. Xing, H. Zhang, and J. Wang, Physical Review Letters **122**, 206401 (2019).

²⁷ G. Xu, H. Weng, Z. Wang, X. Dai, and Z. Fang, Physical Review Letters **107**, 186806 (2011).

²⁸ X.-L. Qi and S.-C. Zhang, Rev. Mod. Phys. **83**, 1057 (2011).

²⁹ Y. Li and F. Haldane, Physical review letters **120**, 067003 (2018).

³⁰ Y. Gong, J. Guo, J. Li, K. Zhu, M. Liao, X. Liu, Q. Zhang, L. Gu, L. Tang, X. Feng, *et al.*, Chinese Physics Letters **36**, 076801 (2019).

³¹ K. Kim, J. Seo, E. Lee, K.-T. Ko, B. Kim, B. G. Jang, J. M. Ok, J. Lee, Y. J. Jo, W. Kang, *et al.*, Nature materials **17**, 794 (2018).

³² C.-Z. Chang, J. Zhang, X. Feng, J. Shen, Z. Zhang, M. Guo, K. Li, Y. Ou, P. Wei, L.-L. Wang, Z.-Q. Ji, Y. Feng, S. Ji, X. Chen, J. Jia, X. Dai, Z. Fang, S.-C. Zhang, K. He, Y. Wang, L. Lu, X.-C. Ma, and Q.-K. Xue, Science **340**, 167 (2013).

³³ X. Wan, A. M. Turner, A. Vishwanath, and S. Y. Savrasov, Physical Review B **83**, 205101 (2011).

³⁴ C. Fang, H. Weng, X. Dai, and Z. Fang, Chinese Physics B **25**, 117106 (2016).

³⁵ H. Weng, Y. Liang, Q. Xu, R. Yu, Z. Fang, X. Dai, and Y. Kawazoe, Physical Review B **92**, 045108 (2015).

³⁶ A. W. Sleight, J. Longo, and R. Ward, Inorganic Chemistry **1**, 245 (1962).

³⁷ P. Giannozzi, S. Baroni, N. Bonini, M. Calandra, R. Car, C. Cavazzoni, D. Ceresoli, G. L. Chiarotti, M. Cococcioni, I. Dabo, *et al.*, Journal of Physics: Condensed Matter **21**, 395502 (2009).

³⁸ P. Giannozzi, O. Andreussi, T. Brumme, O. Bunau, M. B. Nardelli, M. Calandra, R. Car, C. Cavazzoni, D. Ceresoli, M. Cococcioni, *et al.*, Journal of Physics: Condensed Matter **29**, 465901 (2017).

³⁹ J. P. Perdew, K. Burke, and M. Ernzerhof, Physical Review Letters **77**, 3865 (1996).

⁴⁰ D. Vanderbilt, Physical Review B **41**, 7892 (1990).

⁴¹ A. I. Liechtenstein, V. I. Anisimov, and J. Zaanen, Physical Review B **52**, R5467 (1995).

⁴² M. Cococcioni and S. de Gironcoli, Physical Review B **71**, 035105 (2005).

⁴³ C. Lane, J. W. Furness, I. G. Buda, Y. Zhang, R. S. Markiewicz, B. Barbiellini, J. Sun, and A. Bansil, Phys. Rev. B **98**, 125140 (2018).

⁴⁴ Y. Zhang, C. Lane, J. W. Furness, B. Barbiellini, J. P. Perdew, R. S. Markiewicz, A. Bansil, and J. Sun, Proceedings of the National Academy of Sciences **117**, 68 (2020).

⁴⁵ N. Marzari, D. Vanderbilt, A. De Vita, and M. Payne, Physical Review Letters **82**, 3296 (1999).

⁴⁶ A. A. Mostofi, J. R. Yates, Y.-S. Lee, I. Souza, D. Vanderbilt, and N. Marzari, Computer Physics Communications **178**, 685 (2008).

⁴⁷ Q. Wu, S. Zhang, H.-F. Song, M. Troyer, and A. A. Soluyanov, Computer Physics Communications **224**, 405 (2018).

⁴⁸ M. A. Green, A. Hobaillie, and H. J. Snaith, Nature Photonics **8**, 506 (2014).

⁴⁹ N. Rezaei, T. Hashemifar, M. Alaei, F. Shahbazi, S. J. Hashemifar, and H. Akbarzadeh, Phys. Rev. B **99**, 104411 (2019).

⁵⁰ A. Burkov and L. Balents, Physical Review Letters **107**, 127205 (2011).

⁵¹ M. L. Sancho, J. L. Sancho, and J. Rubio, Journal of Physics F: Metal Physics **14**, 1205 (1984).

⁵² N. Marzari, A. A. Mostofi, J. R. Yates, I. Souza, and D. Vanderbilt, Reviews of Modern Physics **84**, 1419 (2012).

⁵³ R. Li, H. Ma, X. Cheng, S. Wang, D. Li, Z. Zhang, Y. Li, and X.-Q. Chen, Phys. Rev. Lett. **117**, 096401 (2016).

⁵⁴ J.-W. Rhim and Y. B. Kim, Phys. Rev. B **92**, 045126 (2015).

⁵⁵ Y.-J. Song and K.-W. Lee, Phys. Rev. B **102**, 035155 (2020).